

Journal of Astronomical Telescopes, Instruments, and Systems

AstronomicalTelescopes.SPIEDigitalLibrary.org

Correction of an active space telescope mirror using a deformable mirror in a woofer-tweeter configuration

Matthew R. Allen
Jae Jun Kim
Brij N. Agrawal

SPIE.

Matthew R. Allen, Jae Jun Kim, Brij N. Agrawal, "Correction of an active space telescope mirror using a deformable mirror in a woofer-tweeter configuration," *J. Astron. Telesc. Instrum. Syst.* **2**(2), 029001 (2016), doi: 10.1117/1.JATIS.2.2.029001.

Correction of an active space telescope mirror using a deformable mirror in a woofer-tweeter configuration

Matthew R. Allen, Jae Jun Kim,* and Brij N. Agrawal

Spacecraft Research Design Center, Naval Postgraduate School, Mechanical and Aerospace Engineering, 700 Dyer Road, Monterey, California 93943, United States

Abstract. The Naval Postgraduate School's segmented mirror telescope (SMT) was developed using prototype silicon carbide active hybrid mirror technology to demonstrate lower cost and rapid manufacture of primary mirror segments for a space telescope. The developmental mirror segments used too few actuators limiting the ability to adequately correct the surface figure error. To address the unintended shortfall of the developmental mirrors, a deformable mirror is added to the SMT and control techniques are developed. The control techniques are similar to woofer-tweeter adaptive optics, where the SMT segment represents the woofer and the deformable mirror represents the tweeter. The optical design of an SMT woofer-tweeter system is presented, and the impacts of field angle magnification on the placement and size of the deformable mirror are analyzed. A space telescope woofer-tweeter wavefront control technique is proposed using a global influence matrix and closed-loop constrained minimization controller. The control technique simultaneously manipulates the woofer and tweeter mirrors. Simulation and experimental results demonstrate a significant improvement in wavefront error of the primary mirror and the control technique shows significant wavefront error improvement compared to sequentially controlling the woofer and tweeter mirrors. © The Authors. Published by SPIE under a Creative Commons Attribution 3.0 Unported License. Distribution or reproduction of this work in whole or in part requires full attribution of the original publication, including its DOI. [DOI: [10.1117/1.JATIS.2.2.029001](https://doi.org/10.1117/1.JATIS.2.2.029001)]

Keywords: segmented mirror telescope; dual-deformable mirror; woofer-tweeter; space telescope; adaptive optics; active optics; wavefront control.

Paper 15074P received Oct. 8, 2015; accepted for publication May 13, 2016; published online Jun. 9, 2016.

1 Introduction

Current earth-imaging satellites operate in low Earth orbit (LEO) and use large monolithic primary mirrors to achieve high-resolution images. LEO limits the time a satellite is in view of a ground target. Increasing the altitude of the satellite increases the time the satellite is in view of the ground target. To achieve similar ground resolution at a higher altitude, the primary mirror's diameter must increase. The primary mirror size required for a medium Earth orbit or geostationary Earth orbit high-resolution imagery satellite is greater than the diameter of available launch vehicle fairings.

The launch vehicle volume and mass constraints impact the space telescope primary mirror design. The volume constraint forces a trade between a monolithic primary mirror and a segmented mirror. A monolithic primary mirror offers a simpler design, but a deployable-segmented mirror allows a primary mirror with a diameter larger than the launch vehicle fairing diameter. The mass constraint impacts primary mirror stiffness and primary mirror optical surface figure. Past space telescope primary mirrors depended on stiffness achieved through structure and mass to maintain their optical surface quality.¹ However, a constraint on mass requires larger primary mirrors to reduce density, thereby reducing stiffness and potentially reducing surface figure performance. The James Webb Space Telescope (JWST) overcomes the mass and volume constraints using a lightweight segmented mirror design with an active wavefront sensing and control system. Similar concepts have

been proposed for visible wavelength (0.4 to 0.7 μm) telescopes using segmented active primary mirrors.

Early active and adaptive optics research considered using active primary mirrors in space telescopes.^{1,2} More recent efforts include the development of the Department of Defense (DoD) segmented mirror telescope (SMT) shown in Fig. 1 and the Advanced Technology Large Aperture Space Telescope (ATLAST)³ conceptual designs. Actuated hybrid mirrors (AHMs) were used for the SMT segments and similar mirrors were proposed for the ATLAST program. The AHM segments are replicated mirrors. The mirrors use a silicon carbide substrate with embedded surface parallel actuators, and a nanolaminate reflective surface. The AHM segments are lightweight, lower cost, and have a shorter manufacturing process than traditional monolithic glass mirrors.⁴

The desired surface figure error for a deployable segment is less than $\lambda/20$ ($\lambda = 633 \text{ nm}$), or less than 32 nm RMS. The SMT AHM segments achieved an average surface figure error of 154 nm RMS using 156 actuators per segment. The AHM manufacturer, Northrup Grumman AOA Xinetics, has since demonstrated average surface figure error of 15.3 nm RMS for 1-m class mirrors using 349 actuators per segment.⁵ AHM technology achieved the desired surface figure error for a future deployable telescope. However, to improve the surface figure error of the SMT test bed, a deformable mirror is added to the optical path to improve the overall performance of the SMT using a two-stage active optics approach.

The combined SMT AHM segments and deformable mirror are similar to a woofer-tweeter adaptive optics system used to compensate for atmospheric turbulence in astronomical

*Address all correspondence to: Jae Jun Kim, E-mail: jki1@nps.edu

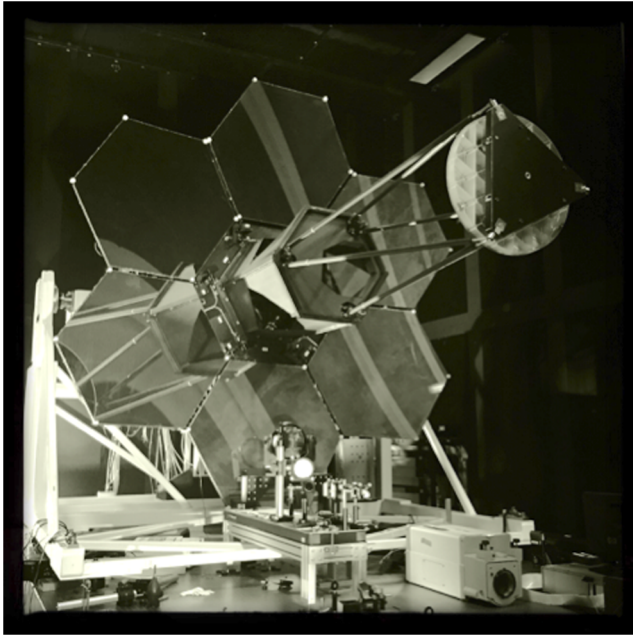


Fig. 1 SMT located at the Naval Postgraduate School.

telescopes and high-energy laser systems. In these systems, the woofer deformable mirror compensates for low spatial and temporal frequency disturbances, and the tweeter deformable mirror compensates for high spatial and temporal frequency disturbances. However, an Earth imaging satellite woofer-tweeter system does not have to correct atmospheric high temporal frequency disturbances, but rather static errors and low frequency disturbances caused by a thermally dynamic environment.^{6,7} The SMT active segment represents the woofer since the resonant frequency is lower than the deformable mirror, and the additional deformable mirror represents the tweeter.

Two-stage deformable mirror systems have also been proposed for space coronagraph missions capable of detecting extra-solar terrestrial planets.⁸ The two-stage deformable mirror system improves contrast by compensating for diffraction caused by the aperture and amplitude aberrations caused by the telescope optics. For example, the WFIRST-AFTA instrument uses a two deformable mirror control system to improve contrast performance by compensating for aperture discontinuities.⁹ Several coronagraph wavefront control techniques have been proposed. Shaklan and Green⁸ control phase using one deformable mirror and amplitude using the other deformable mirror. Pueyo et al.¹⁰ use a stroke minimization technique that allows the deformable mirrors to be simultaneously commanded while improving the coronagraph contrast.

In this paper, we describe the design approach to add a deformable mirror to the SMT optical assembly in order to improve the surface figure error of the SMT. Section 2 introduces the SMT and Sec. 3 describes the space telescope woofer-tweeter design approach using the SMT as an example. Section 4 describes modeling both the SMT and the additional deformable mirror. A space telescope woofer-tweeter control approach is presented in Sec. 5 and simulation and experimental results are presented in Sec. 6. The simulation and experimental results show the feasibility of using adaptive optics to improve the optical performance of a large aperture imagery satellite and the ability to trade optical surface requirements between the primary mirror segments and a deformable mirror.

2 Segmented Mirror Telescope Background

The SMT is a 3-m deployable-segmented telescope with six hexagonal active 1-m segments. Developed by the DoD, the SMT demonstrated critical SMT technologies including light-weight active mirrors, deployment mechanisms, and wavefront sensing and control technologies. Figure 2 shows the SMT optical layout.

The SMT uses a wavefront sensing and control system to move the segments from their post deployment unphased positions to their operational diffraction limited position. The control system improves the wavefront error from several millimeters to below the diffraction limit using three control modes. The wavefront sensing and control system first coarsely align the segments, then coarsely phase the segments, then finely phase the segments and improve the segment surface wavefront error. Redding et al.¹² present a similar approach using the JWST as an example.

The SMT segments are adjusted using three types of actuators and serve as the control system inputs. Each segment has 156 lead magnesium niobate (PMN) electrostrictive face sheet actuators (FSAs) embedded into the segment ribbing parallel to the surface. Figure 3 shows the FSA locations on the segment ribs. The FSAs correct the surface of the segment. Each segment is attached to three PMN fine control actuators (FCAs). These FCAs adjust for segment piston, tip, and tilt. Each FCA is connected to a bipod. Each leg of the bipod is a coarse control actuator (CCA) and is attached to the primary mirror support structure. There are six CCAs per segment and they are used like a hexapod to coarsely align the segments after deployment. Figure 4 shows the locations of the CCAs and FCAs on the back of a segment.

The SMT wavefront sensing system consists of a Shack–Hartmann wavefront sensor and a phase diversity wavefront sensor. The two wavefront sensors are used to measure phase and provide feedback to the controller to perform coarse phasing and fine phasing. The initial wavefront error after telescope

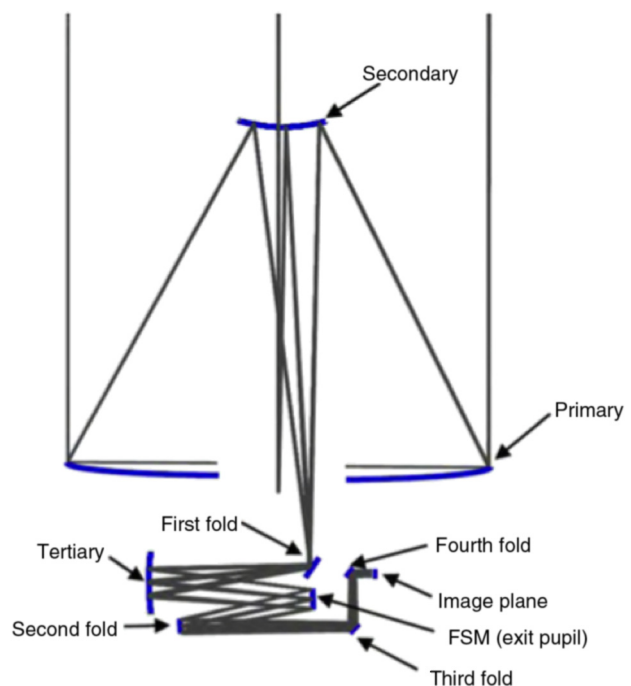


Fig. 2 SMT optical layout.¹¹

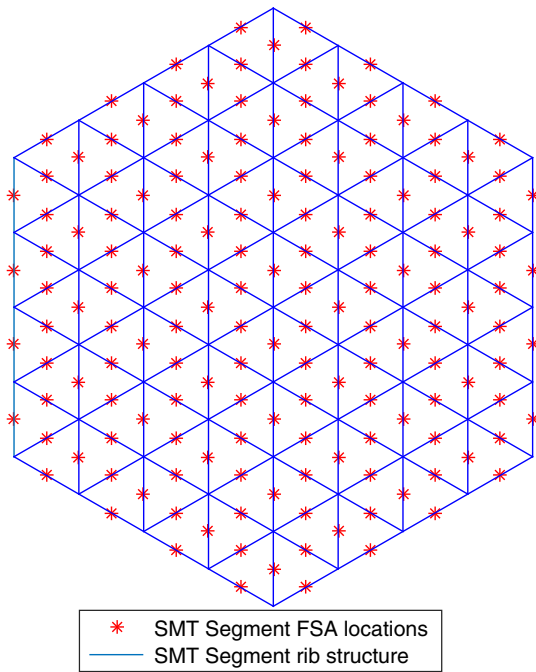


Fig. 3 FSA locations on SMT segment.

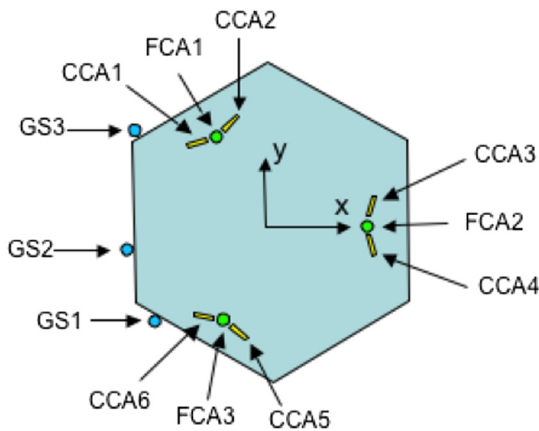


Fig. 4 SMT segment CCA, FCA, and gap sensor (GS) locations.

deployment is outside the capture range of the wavefront sensors. Three gap sensors are used on each segment to measure displacements between adjacent segments and coarsely align the segments within the capture range of the wavefront sensors. Figure 4 shows the location of the gap sensors on a segment.

The wavefront control system uses the gap sensor measurements and phase measurements as feedback to command the actuators to align and phase the segments. Table 1 shows the three control modes with their associated inputs, outputs, and sample rates. The gap sensors provide feedback for coarse alignment of the segments. The coarse phasing control uses gap sensor feedback at 1 kHz and phase diversity sensor data at 1 Hz to remove gap sensor bias. The fine phasing control uses two feedback controllers. The Shack–Hartmann sensor output and the FSA controller correct the surface of the segments. The phase diversity sensor output and FCA controller maintain segment phasing by finely controlling segment tip, tilt, and piston.

Table 1 Control modes.

Control mode	Sample rate (Hz)	Outputs	Inputs
Coarse alignment	0.1	Gap sensor	CCAs
Coarse phasing	1000	Gap sensor, phase diversity sensor	FCAs
Fine phasing	200	Shack–Hartmann	FSAs
	1	Phase diversity sensor	FCAs

The SMT test bed has inherent problems that prevent the current control architecture from phasing the six segments. First, the gap sensors do not have enough accuracy to measure segment displacements to within the capture range of the wavefront sensors. Newer SMT concepts use a laser truss metrology system to align and maintain a segmented telescope wavefront and avoid using gap sensors.¹³ The second SMT problem is vibration caused by the latches connecting the segments to the support structure. These vibrations cause large optical path length changes between segments preventing the segments from being phased.¹¹ Despite these problems, the SMT is still a useful experimental test bed allowing research in the control of structural vibrations and wavefront sensing and control.

The SMT is a steerable field of view (FOV) system with a 0.5×0.5 deg telescope field of view (TFOV) and the focal plane has a 2×2 arcmin FOV. The SMT uses a fast steering mirror (FSM) to steer the focal plane FOV within the TFOV. Figure 5 shows the focal plane FOV within the TFOV.

The SMT active segments have surface errors after correction consisting of high spatial frequency print-through. The FCA fixture points on the back of the segments also cause larger low spatial frequency errors. Figure 6 shows the optical path difference (OPD) of an SMT AHM segment measured in waves after correction, and a fast Fourier transform (FFT) log plot identifying the prominent spatial frequencies. The residual OPD plot shows a phase discontinuity near the center of the segment. This discontinuity is due to an imperfection in the segment surface and is found in all six segments. These center imperfections

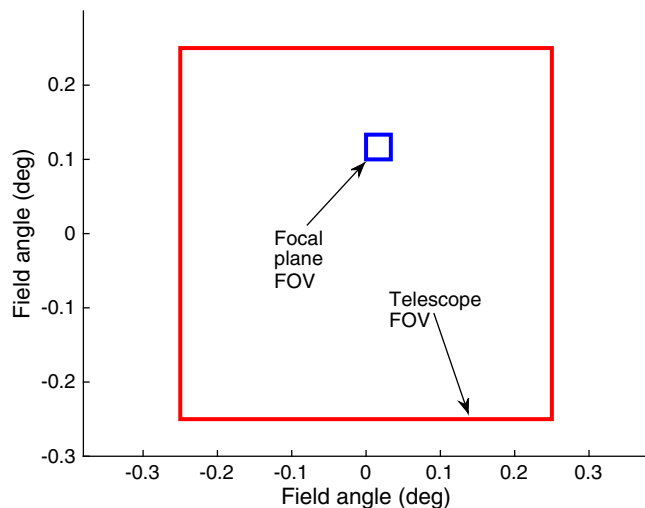


Fig. 5 TFOV and focal plane FOV.

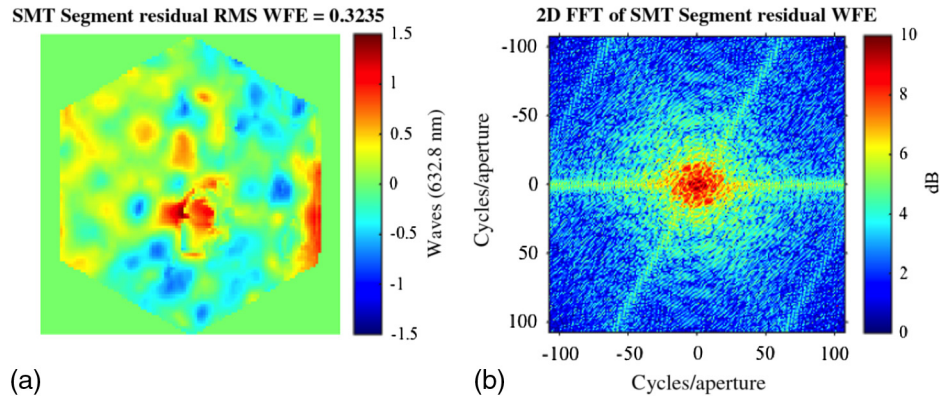


Fig. 6 (a) SMT segment residual OPD in waves and (b) 2-D FFT log plot of SMT residual surface error.¹⁴

are not original to the AHM segments, but were caused during the FCA replacement process when upgrading the FCAs to a newer actuator. The segment FSAs are unable to completely remove these errors because the actuators do not have enough stroke and there are too few actuators to remove all the spatial frequencies. While newer AHM mirrors have much better performance as discussed in Sec. 1, the addition of a deformable mirror to the SMT optical assembly in a woofer-tweeter configuration can improve these errors.

3 Segmented Mirror Telescope Woofer-Tweeter Design Approach

The SMT woofer-tweeter system design has four key assumptions. First, the wavefront disturbances are low frequency allowing the two mirrors to operate at the same bandwidth. Second, the wavefront sensing system measures the combined wavefront error of the primary mirror and the additional deformable mirror. Third, the individual segments are phased relative to each other and piston, tip, or tilt error is removed using the individual segment coarse and fine actuators. Fourth, the SMT AHM segment and deformable mirror responses are designed to be linear, and the actuator responses obey the principle of linear superposition.

The natural placement of the deformable mirror is at the exit pupil because all field angles are present and it is the conjugate to the primary mirror. Figure 7 shows the deformable mirror at

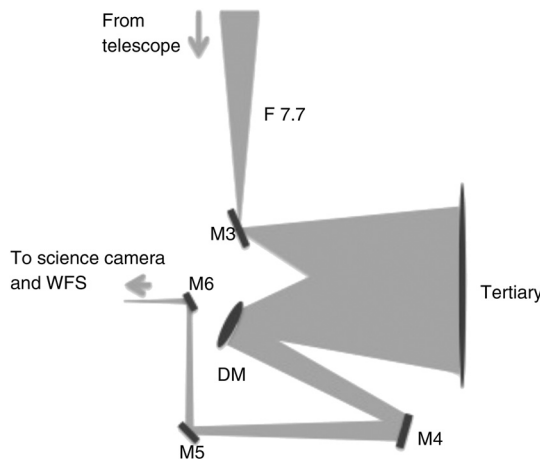


Fig. 7 SMT optical layout replacing the FSM with a deformable mirror on a gimbal.¹⁵

the exit pupil and requires the mirror size to match the exit pupil diameter. However, the FSM resides at the exit pupil. The FSM functionality can be maintained using a gimballed deformable mirror. Another option is to relay the exit pupil after the FSM and reduce the size of the exit pupil to accommodate a smaller deformable mirror, shown in Fig. 8.

The SMT exit pupil is demagnified 20 \times to a diameter of 150 mm; this has the effect of magnifying the field angles 20 \times due to the Lagrange invariant. Adding the pupil relay to accommodate a 25-mm commercially available deformable mirror magnifies the field angles by 120 \times . The field angles at the deformable mirror are represented by

$$\theta_{DM} = M_{\alpha}\theta_{PM}, \quad (1)$$

where the angular magnification is represented as M_{α} and θ_{PM} is field angle at the primary mirror.¹⁶

McComas and Friedman¹⁶ used the field angle relationship to describe the residual path length error of a space telescope with a deformable mirror, represented by

$$\phi(x, y) = 2d_{PM}(x, y) \cos(\theta_{PM}) - 2d_{DM}(x, y) \cos(M_{\alpha}\theta_{PM}). \quad (2)$$

The residual path length error is the difference between the path length error caused by the primary mirror

$$\phi_{PM}(x, y) = 2d_{PM}(x, y) \cos(\theta_{PM}), \quad (3)$$

and the correction applied by the deformable mirror

$$\phi_{DM}(x, y) = 2d_{DM}(x, y) \cos(M_{\alpha}\theta_{PM}). \quad (4)$$

The variable d_{PM} is the surface distance of the primary mirror relative to the nominal position. The variable d_{DM} is the surface distance of the deformable mirror from the flat position. Equation (4) can be used to size the deformable mirror diameter and mirror stroke to correct for the primary mirror surface error at off axis TFOV locations.

The result of Eq. (2) is that depending on the angular magnification, the deformable mirror may not correct all the field angles as the term $M_{\alpha}\theta_{PM}$ approaches $\pi/2$. Figures 9 and 10 show the additional correction in waves required by the deformable mirror for the 20 \times and 120 \times field angle cases, respectively, given 1 wave of error on the primary mirror. Figure 9 shows that at far-field angles, the additional error correction required is negligible. However, Fig. 8 shows that at far-field angles, an

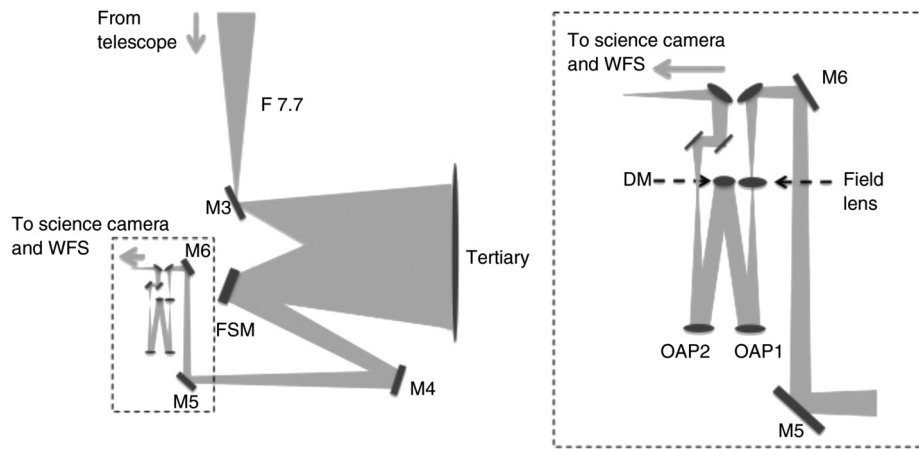


Fig. 8 SMT optical layout with deformable mirror optical relay and pupil size reduced.¹⁵

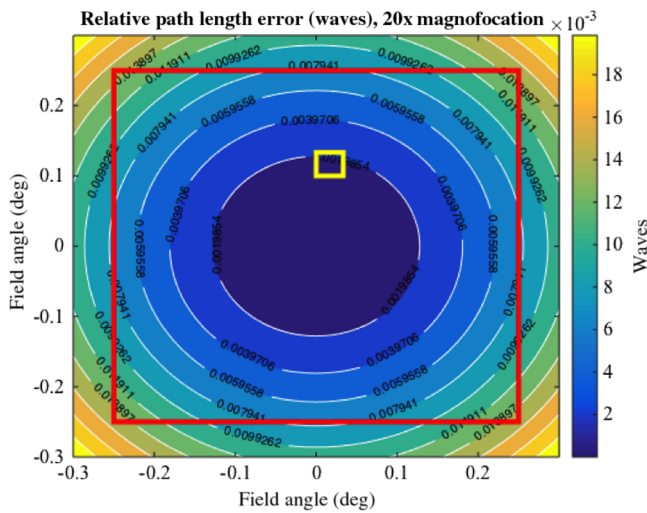


Fig. 9 Relative path length error (waves) for 20x angular magnification.

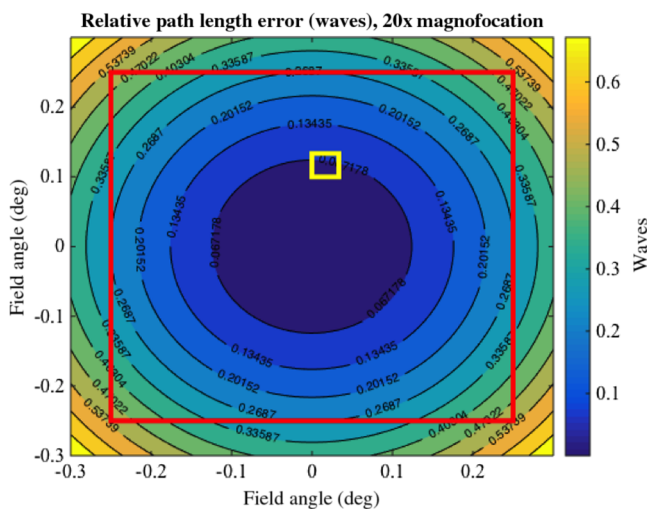


Fig. 10 Relative path length error (waves) for 120x angular magnification.

additional half wave of correction is required to correct 1 wave of error on the primary mirror. In both examples, the term $M_\alpha \theta_{PM}$ does not approach $\pi/2$ over the TFOV and the deformable mirror can compensate for field angle magnification at the edge of the TFOV. However, the mirror stroke must be sized for the anticipated primary mirror surface error and the field angle magnification at off axis TFOV locations.

The field angle relationship is not the only limitation of the woofer-tweeter deformable mirror concept. Another consideration is pupil shear and pupil distortion. Pupil shear and pupil distortion can cause the mapping of the primary mirror to the deformable mirror to vary with the field, requiring different field angle corrections at similar field angles throughout the TFOV. The best solution when using active optics with a wide FOV telescope is to have a high-quality primary mirror without a deformable mirror. However, if a deformable mirror is used, a larger diameter deformable mirror is preferred with a small angular magnification. If a smaller deformable mirror is used, different actuators for each field positions can be used to account for pupil shear and pupil distortion effects at the deformable mirror.

4 Segmented Mirror Telescope Woofer-Tweeter Modeling and Control

A single SMT segment is used to model and experimentally demonstrate the woofer-tweeter concept because of the phasing challenges discussed in Sec. 2. The single SMT segment approach is valid because fine phasing is accomplished after phasing the segment edges in the wavefront sensing and control approach. The fine phasing modeled in this section only applies to segment surface control using the FSAs. Using a single segment reduces the complexity and size of the model and is extendable to the entire six segment aperture.

The SMT woofer-tweeter system model combines an SMT quasistatic state space model and a surface normal deformable mirror model. The model output is the sum of the two mirror OPDs and the input is a vector of actuator inputs. The response bandwidths of the mirrors are assumed to be the same because the sensor is much slower than the response bandwidth of the mirrors. Areas of the deformable mirror are mapped to an SMT segment to individually correct the residual error of the segments. The model can correct the segment residual surface using the SMT FSA actuators and deformable mirror actuators by commanding the respective actuators in series or parallel.

The SMT model uses simulated Shack–Hartmann sensor outputs to reconstruct the wavefront of the segments and recombines the segments to form the entire six segment aperture.

A second-order dynamic SMT state space model was developed from a finite element model (FEM) of the segments and the optical telescope assembly. To reduce model computational complexity, the normal eigenmodes within the frequency band of interest were extracted from the FEM and the high frequency modes were truncated. The truncated high frequency modes are associated with the segment FSAs' response. To capture the FSA modes, the eigenmodes were augmented with additional residual modes. The second-order state space model is represented by

$$\{\dot{x}(t)\} = [A]\{x(t)\} + [B]\{u(t)\}, \quad (5)$$

and

$$\{y_{\text{SMT}}(t)\} = [C]\{x(t)\} + [D]\{u(t)\} \quad (6)$$

using generalized modal coordinates

$$\{x\} = \begin{Bmatrix} q \\ \dot{q} \end{Bmatrix} \quad (7)$$

and actuator input vector $\{u\}$. The A matrix represents the modal frequencies and the B matrix represents the mode sensitivity to actuator inputs. The vector $\{y\}$ is a vector representation of the OPD output of the telescope wavefront. The matrix C represents the mode shapes at the sensor locations and the D matrix statically represents the high frequency modes associated with the FSA response. An analytical static influence matrix model is found from the dynamic model by assuming a steady state response, $\{\dot{x}(t)\} = 0$

$$\{x(t)\} = -[A]^{-1}[B]\{u(t)\}. \quad (8)$$

Substituting Eq. (8) into Eq. (6) directly relates the outputs to the inputs

$$\{y_{\text{SMT}}(t)\}_{\text{Steady_state}} = -[C][A]^{-1}[B]\{u(t)\} + [D]\{u(t)\}. \quad (9)$$

Equation (10) is then the analytical influence matrix and Eq. (11) is the SMT quasistatic model assuming the telescope structural dynamics are slow compared to the FSA response and the disturbance bandwidth is low frequency ($f \ll 1$ Hz).

$$\Gamma = [D] - [C][A]^{-1}[B], \quad (10)$$

$$\{y_{\text{SMT}}(t)\}_{\text{Steady_state}} = \Gamma_{\text{SMT}}\{u_{\text{SMT}}(t)\}. \quad (11)$$

The quasistatic approach simplifies the control of the segment face sheets. The model is further reduced to a single segment by selecting the segment outputs, segment FSA inputs, and columns of the influence matrix associated with the specific segment.

The deformable mirror analytical model is an influence matrix comprised of influence functions that relate the mirror surface response to the actuator inputs

$$\{y_{\text{DM}}\} = [\Gamma_{\text{tweeter}}]\{u_{\text{DM}}\}. \quad (12)$$

The influence functions are modeled as Gaussian functions¹⁷ and the actuator spacing is set to match the highest dominate spatial frequency identified using the two-dimensional (2-D) FFT plot of the primary mirror segment. In Sec. 5, the analytical model is replaced with an experimental model that uses an experimentally derived influence matrix.

The woofer-tweeter system is controlled using a global influence matrix by concatenating the woofer influence matrix and tweeter influence matrix into one matrix. This is possible because the SMT segment influence matrix and deformable mirror influence matrix have the same number of rows since the mirror responses are measured and reconstructed from the same wavefront sensing system. The result is a single global influence matrix for the woofer-tweeter system

$$\Gamma_G = [\Gamma_{\text{SMTSegment}} \quad \Gamma_{\text{Tweeter}}]. \quad (13)$$

Feedback control is used to command the woofer-tweeter system because of uncertainty and disturbances in the system. An iterative constrained optimization approach minimizes the wavefront while ensuring the control signals remain within the limits of the actuators.¹⁴ A single step linear model

$$\{\phi\} = [\Gamma_G]\{u\} + \{\phi_0\} \quad (14)$$

represents the system. The output is in terms of the wavefront measured in OPD, $\{\phi\}$, and $\{\phi_0\}$ is the wavefront that represents the initial condition. The constrained minimization approach uses the quadratic cost function

$$\begin{aligned} \text{argmin } J(u) &= \frac{1}{2} [([\Gamma_G]\{u\} + \{\phi_0\})^T ([\Gamma_G]\{u\} + \{\phi_0\})] \\ &\text{subject to: } lb \leq u \leq ub \end{aligned} \quad (15)$$

subject to constraints on the lower bounds and upper bounds of available control to find the control voltage that minimizes the wavefront error. The feedback controller updates the control signal, u_{k+1} , iteratively using the solution to the constrained minimization

$$\{u_{k+1}\} = \mu\{u_{c,k}\} + \{u_k\}. \quad (16)$$

At each iteration, the constrained minimization is solved with new lower and upper bounds represented by $u_{c,k}$. The gain μ is between 0 and 1.

To predict the performance of the woofer-tweeter system for varying tweeter actuator counts, the woofer-tweeter global iterative constrained minimization controller is used. The actuators of the tweeter are modeled over an evenly spaced square grid and actuators without influence over the SMT segment are removed. To effectively compensate for the SMT segment surface error, the actuator spacing needs to match the highest dominant spatial frequency. Treating the actuator grid size as a variable, Fig. 11 shows the RMS wavefront error versus the number of tweeter actuators. The wavefront error attributed to the SMT segment can be significantly improved using a deformable mirror. Figure 12 compares the simulated surface plots of the SMT AHM segment before and after the woofer-tweeter controller is applied. The simulated 471 deformable mirror actuators and the SMT segment actuators remove the

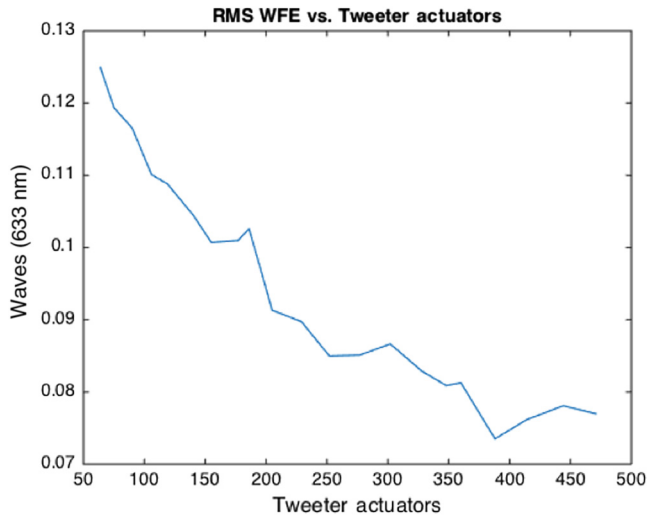


Fig. 11 SMT woofer-tweeter RMS wavefront error versus the number of tweeter actuators.

SMT segment print through and significantly improve the center imperfection.

5 Experimental Setup, Simulation, and Results

Experimentally testing a large optical system like the SMT presents challenges. This section describes how the woofer-tweeter concept was demonstrated using the SMT test bed. The model and controller from Sec. 4 were updated using experimentally derived influence functions for both the SMT segment and the deformable mirror. The simulated results are compared to the experimental results showing agreement.

The primary testing challenge was the lack of a large diameter collimated reference light source. This prevented the use of the SMT wavefront sensors as described in Sec. 2. To overcome this, a center of curvature test was used with a laser interferometer to measure the surface error of the SMT primary mirror. A deformable mirror was added to the center of curvature

test at the pupil plane using relay optics. The pupil plane was demagnified to 6.75 mm. The center of curvature laser interferometer test bed was a valid approach to demonstrate the woofer-tweeter control concept because the interferometer measures the same primary mirror surface errors as the SMT wavefront sensors, the primary mirror is the largest contributor of wavefront error, and the deformable mirror is located at a pupil as discussed in Sec. 3.

Two main differences between the experimental setup and the intended SMT operations were the interferometer bandwidth and the lack of field steering. The interferometer was configured to operate at 1 Hz, while the Shack–Hartmann wavefront sensor was configured to operate at 200 Hz. The slower interferometer still allowed for closed-loop control in the laboratory environment where external disturbances are minimal. Field steering was not demonstrated and all experiments were conducted on the primary axis. However, in Sec. 2 we showed that given a proper sized deformable mirror angular magnification of primary mirror errors can be corrected.

Figure 13 shows the deformable mirror added to the center of curvature test in a double pass configuration. The test setup uses a 4D Technologies Corp. PhaseCam 4020 laser interferometer with an $f/3$ diverging lens, a null corrector, and a hexapod to align the interferometer to the SMT optical axis. A Boston Micromachines Corporation (BMC) continuous surface 140-actuator deformable mirror with a 3.3 mm \times 3.3 mm square aperture and 1.8 μ m of stroke is used as the tweeter.

The pupil plane of the primary mirror relays from the $f/3$ objective to the deformable mirror and then relays it to the interferometer. A single SMT segment pupil fits on the deformable mirror in the optical setup. The BMC deformable mirror actuators are experimentally mapped to the SMT segment with 61 actuators having measured influence over on the SMT segment wavefront.

The SMT woofer-tweeter simulation was updated to match the experimental setup using an experimentally derived global influence matrix with zero mean Gaussian plant noise. The sensor model used the OPD output from the woofer-tweeter model and added zero-mean Gaussian noise to represent the

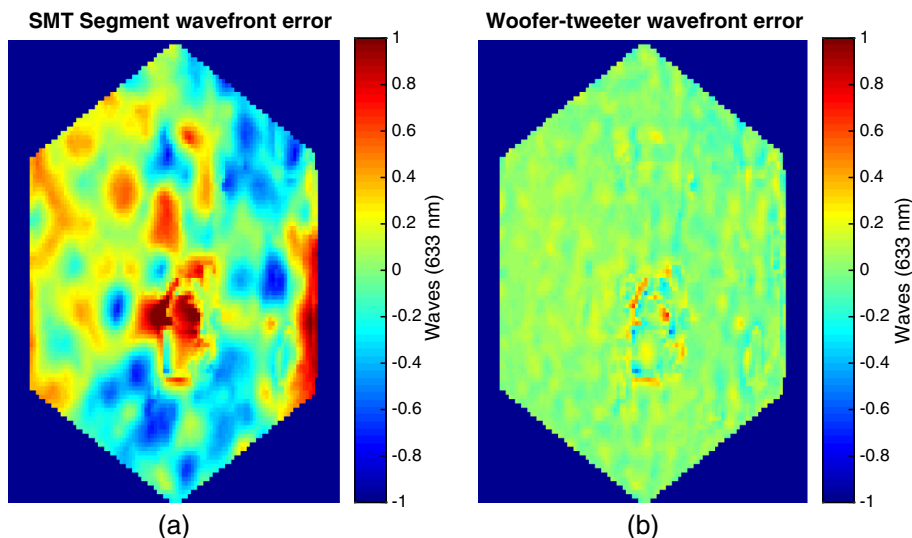


Fig. 12 (a) SMT RMS wavefront error 0.32 waves and (b) SMT woofer-tweeter wavefront error 0.07 waves using 471 actuators.

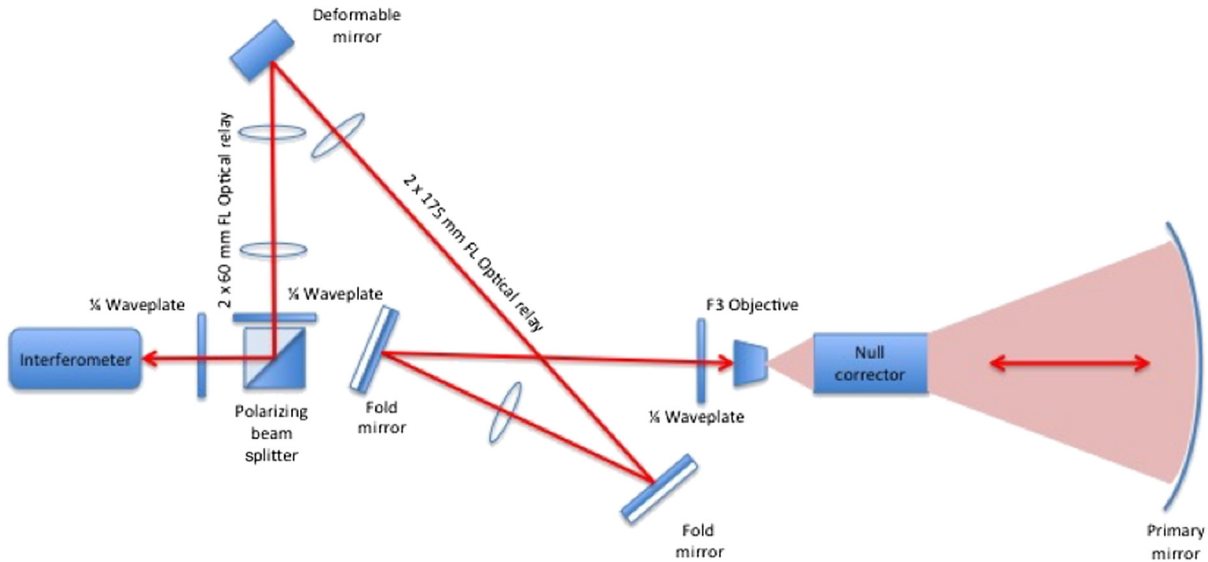


Fig. 13 SMT center of curvature test with deformable mirror and pupil relay optics.

laser interferometer output. The simulations used a static bias as an initial condition.

Figure 14 shows the mean error history and standard deviation for three simulations. The first simulation used an iterative constrained minimization controller to control the SMT woofer. The second simulation used two sequential iterative constrained minimization controllers to correct the woofer and then correct the tweeter. The third simulation used the global iterative constrained minimization controller to simultaneously manipulate the woofer and tweeter. The simulated results show that the combined global iterative minimization control approach outperformed the sequential control approach. The sequential woofer-tweeter controller under performance was due to the initial condition of each controller. The wavefront error after applying the woofer controller portion of the sequential controller had high spatial frequency errors that were not present at the SMT biased position. The BMC-140 tweeter did not have enough actuators to correct the high spatial

frequency errors. However, by combining the woofer and tweeter into a global influence matrix, the mirrors collectively corrected higher spatial frequencies.

Figure 15 shows experimental wavefront error history for three cases previously simulated. The experimental results validated the woofer-tweeter models and show an improved wavefront error correction by controlling the woofer and tweeter simultaneously rather than separately. Figure 14 shows a simulated final RMS wavefront error of 0.213 waves and Fig. 15 shows the experimental system achieved a final RMS wavefront error of 0.201 waves where the last five iterations show the system reaching steady state as there is no change. Figure 16 shows the final wavefront for the three cases. The woofer-tweeter control approach reduced the peak-to-valley wavefront error more than the other cases and improved the lower spatial frequencies. This is expected since the experimental tweeter does not have the actuator density required to remove the high spatial frequencies.

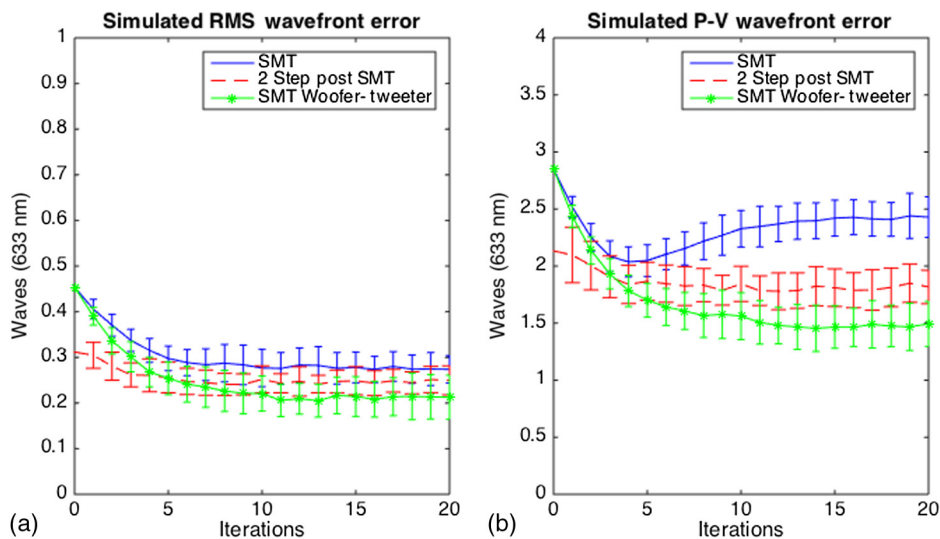


Fig. 14 Simulated SMT and SMT woofer-tweeter wavefront error history using an iterative constrained minimization controller, (a) RMS wavefront error and (b) peak-to-valley wavefront error.

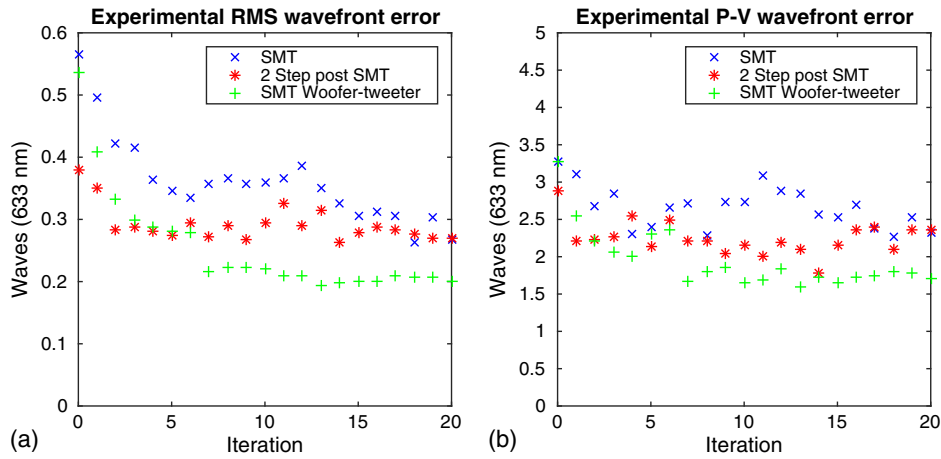


Fig. 15 Experimental SMT and SMT woofer-tweeter wavefront error history using an iterative constrained minimization controller, (a) RMS wavefront error and (b) peak-to-valley wavefront error.

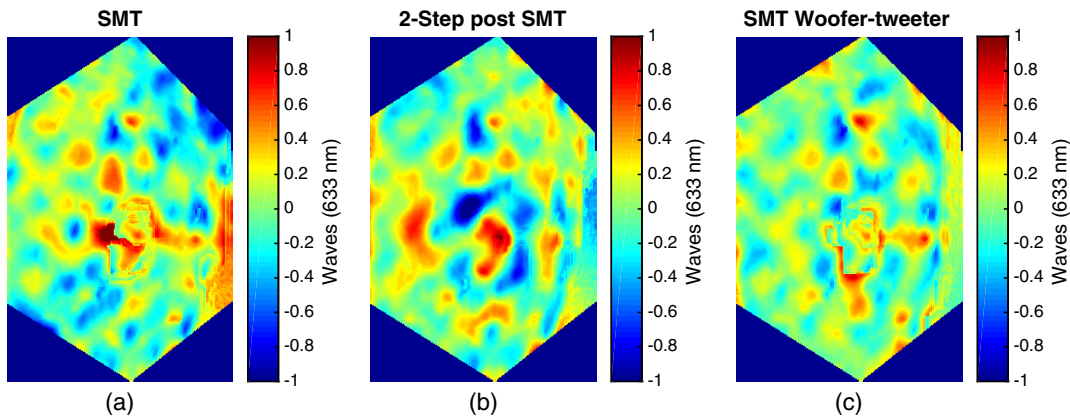


Fig. 16 (a) Experimental SMT wavefront error 0.32 waves RMS, (b) two-step post SMT wavefront error 0.27 waves RMS, (c) and SMT woofer-tweeter wavefront error 0.20 waves RMS.

The results show that a space telescope woofer-tweeter system is viable and can improve the wavefront error attributed to a primary mirror segment. The experimental woofer-tweeter performance was limited by the number of the deformable mirror actuators; however, a 35% RMS wavefront error and 30% peak-to-valley wavefront error improvement was shown. Additionally, a 25% RMS wavefront error improvement and 26% peak-to-valley wavefront error improvement was shown by controlling the woofer and tweeter together rather than controlling them sequentially.

6 Conclusion

A space telescope woofer-tweeter design concept was developed to compensate for surface error of a telescope using a segmented active primary mirror. The impacts of field angle magnification on the placement and size of an additional deformable mirror were analyzed using the SMT as an example. A quasistatic woofer-tweeter model and control approach were developed. The woofer-tweeter system and control approach were simulated and experimentally validated using the SMT center of curvature test bed with a deformable mirror.

This research showed the feasibility of including a deformable mirror in a space telescope with a lightweight active primary mirror and the ability to control the mirrors and reduce

wavefront errors associated with the primary mirror. While this paper focused on correcting a poor-quality active primary mirror, more recent active primary mirrors do not require additional correction.^{4,5} However, deformable mirrors may still be used for figure control in space telescopes including the correction nonactive primary mirrors for both monolithic and segmented designs. Future space telescope coronagraph missions also plan to use deformable mirrors to compensate for phase and amplitude.

Acknowledgments

The authors would like to acknowledge Dr. Bautista Fernandez and Dr. John Bagnasco of Naval Postgraduate School, Dr. Ty Martinez of the Naval Research Laboratory, and Dr. David Redding of the Jet Propulsion Laboratory for their contributions to the SMT test bed development and testing.

References

1. W. E. Howell, "Recent advances in optical control for large space telescopes," in *Space Optics—Proc. of the Ninth Int. Congress of the Int. Commission for Optics (ICO IX)*, pp. 239–258, National Academies (1974).
2. J. W. Hardy, "Active optics: a new technology for the control of light," *Proc. IEEE* **66**(6), 651–697 (1978).

3. M. Postman et al., "Advanced technology large-aperture space telescope: science drivers and technology developments," *Opt. Eng.* **51**(1), 011007 (2012).
4. G. Hickey et al., "Actuated hybrid mirrors for space telescopes," *Proc. SPIE* **7731**, 773120 (2010).
5. J. Wellman and D. Blaszkak, *Advanced Active Hybrid Mirrors for Segmented Space Telescopes*, Naval Postgraduate School, Monterey, California (2012).
6. T. R. O' Meara, C. J. Swigert, and W. P. Brown, "Adaptive optics for space telescopes," *Proc. SPIE* **0075**, 126–135 (1976).
7. T. L. Gray et al., "Minimizing high spatial frequency residual error in active space telescope mirrors," *Proc. SPIE* **7436**, 74360M (2009).
8. S. B. Shaklan and J. J. Green, "Reflectivity and optical surface height requirements in a broadband coronagraph 1Contrast floor due to controllable spatial frequencies," *Appl. Opt.* **45**(21), 5143 (2006).
9. J. Mazoyer et al., "Active compensation of aperture discontinuities for WFIRST-AFTA: analytical and numerical comparison of propagation methods and preliminary results with a WFIRST-AFTA-like pupil," *J. Astron. Telesc. Instrum. Syst.* **2**(1), 011008 (2015).
10. L. Pueyo et al., "Optimal dark hole generation via two deformable mirrors with stroke minimization," *Appl. Opt.* **48**(32), 6296 (2009).
11. A. Yingling, "Integrated optics, structures, and controls of segmented mirror telescopes," Dissertation, Naval Postgraduate School (2012).
12. D. C. Redding et al., "Wavefront sensing and control for large space optics," in *2003 IEEE Aerospace Conf.*, Vol. **4**, pp. 1729–1744 (2003).
13. D. C. Redding et al., "Active optics for a 16-meter advanced technology large aperture space telescope," Jet Propulsion Laboratory, California Institute of Technology (2008).
14. M. R. Allen, J. J. Kim, and B. N. Agrawal, "Correction of active space telescope mirror using woofer-tweeter adaptive optics," *Proc. SPIE* **9469**, 946902 (2015).
15. D. T. Gavel, "Adaptive optics sensing and control development: final report on collaborative research with naval postgraduate school adaptive optics controls laboratory," University of California Observatories (2011).
16. B. K. McComas and E. J. Friedman, "Field-balanced adaptive optics error function for wide field-of-view space-based systems," *Opt. Eng.* **41**(3), 567–574 (2002).
17. R. K. Tyson and B. W. Frazier, *Field Guide to Adaptive Optics*, 2nd ed., SPIE Press, Bellingham, Washington (2012).

Matthew R. Allen is a graduate of the Naval Postgraduate School and received his master's and PhD degree in astronautical engineering in 2007 and 2015. He also received his bachelor of science in chemical engineering from Rensselaer Polytechnic Institute in 2000. His dissertation research focused on wavefront control techniques for large aperture segmented space telescopes.

Jae Jun Kim is a research associate professor at the Naval Postgraduate School. His teaching interests include mechanical vibration, dynamics and control of flexible spacecraft, and acquisition, tracking, and pointing of military spacecraft. His research interests include using active and adaptive optics for large aperture telescopes and imaging spacecraft, and high energy laser beam control.

Brij N. Agrawal is a distinguished professor, director of the Spacecraft Research and Design Center, and director of the Adaptive Optics Center of Excellence for National Security at the Naval Postgraduate School. His teaching interests include acquisition, tracking, and pointing of military spacecraft, spacecraft dynamics and control, and spacecraft design. His current research interests include acquisition tracking and pointing of flexible spacecraft with optical payloads and high energy laser beam control.